# Dark spatial solitons of the TM type

Yijiang Chen
*Optical Sciences Centre, Australian National University, Canberra, Australian Capital Territory 2601, Australia*
(Received 11 June 1991)

The existence of dark spatial solitons of the TM type is examined. This type of two-dimensional solitary wave is found to exist in the self-defocusing nonlinear medium of a Kerr-law type in the range of the wave effective index $n_{\text{eff}}$ from $0.82n_0$ to $n_0$ of the linear refractive index of the medium. This contrasts with dark spatial solitons of the TE type, which exist in the range of $n_{\text{eff}}$ from 0 to $n_0$. The longitudinal component is shown to play a key role leading to this distinction. The comparison between TM and TE solitons is also made on other aspects. For example, the field profile of the TM soliton is shown to vary with the wave effective index, whereas that of the TE soliton is characterized by the hyperbolic tangent function, independent of $n_{\text{eff}}$.

PACS number(s): 42.65.Jx, 42.50.Qg, 42.65.Bp

## I. INTRODUCTION

Spatial solitons are the stable formation of self-guided beams propagating in homogeneous nonlinear media [1–15]. Trapped in a self-focusing nonlinear medium, a stable self-guided beam is referred to as a bright spatial soliton on account of its convex intensity profile which induces a convex refractive index profile for self-guidance, whereas that trapped in a self-defocusing nonlinear medium is referred to as a dark spatial soliton on account of its concave intensity profile which induces a convex index profile for self-guidance. A self-guided beam is a mode of the optical waveguide it induces [11,15]. Therefore, as in a linear waveguide [16,17], the self-induced waveguide could support TE and TM mode patterns. Indeed, it has been shown that trapping in a self-focusing nonlinear medium can occur in these patterns [1,4–9] for any beam effective index $n_{\text{eff}}$ (defined as the wave propagation constant $\beta$ divided by $k$ of the wave number) greater than $n_0$ of the linear refractive index of the medium. For a self-defocusing nonlinear medium, the TE mode pattern has been predicted [10] and experimentally observed [12–14] to be a trapped light pattern for all the possible values of $n_{\text{eff}}$ ranging from 0 to $n_0$. Naturally, it is tempting to know whether light trapping in a self-defocusing nonlinear medium is possible in the form of the TM pattern. In this paper, we will show that a two-dimensional TM beam can indeed be a trapped light pattern in the self-defocusing nonlinear medium of a Kerr-law type. But the self-guidance in this pattern is limited to the range of the wave effective index $n_{\text{eff}}$ from $0.82n_0$ to $n_0$, in contrast with the TE type that exists for all possible values of $n_{\text{eff}}$ ranging from 0 to $n_0$.

## II. WAVE EQUATIONS AND INEXISTENCE OF GRAY SPATIAL SOLITONS

The refractive index in a self-defocusing nonlinear medium decreases with increasing electric-field intensity. For a Kerr-law nonlinearity, the refractive index $n^2$ of a homogeneous medium relies on the field intensity $|E|^2$ linearly,

$$n^2=n_0^2-n_0n_2|\mathbf{E}|^2 , \tag{1}$$

with $n_2$ a positive constant, depending on materials. A light wave propagating in a medium obeys Maxwell's equations which, in terms of the electric field alone, read

$$\nabla\times\nabla\times\mathbf{E}+\frac{1}{c^2}\frac{\partial^2}{\partial t^2}(n^2E)=\mathbf{0} , \tag{2}$$

with $c$ the speed of light in free space. The stationary propagation of the TM wave (cw) along the longitudinal distance $z$ stipulates the field $\mathbf{E}$ to have the functional from of

$$\mathbf{E}(x,z,t)=[e_x(x)\hat{\mathbf{x}}+e_z(x)\hat{\mathbf{z}}]e^{i(\beta z-\omega t)} , \tag{3}$$

where $\omega$ denotes the frequency of a cw. Substitution of this $\mathbf{E}$ into Eq. (2) with the specified $n^2$ of eq. (1) leads to two coupled diffeential equations governing the components $e_x$ and $e_z$,

$$\Psi_x''+\Psi_x-(|\Psi_x|^2+|\Psi_z|^2)\Psi_x=\frac{2b^2}{1-b^2(|\Psi_x|^2+|\Psi_z|^2)}\left\{\Psi_x[\mathrm{Re}(\Psi_x^*\Psi_x''+\Psi_z^*\Psi_z'')+|\Psi_z'|^2+|\Psi_x'|^2]+\Psi_x'\mathrm{Re}(\Psi_x'\Psi_x^*+\Psi_z'\Psi_z^*)\right.$$
$$\left.+\frac{2b^2[\mathrm{Re}(\Psi_x^*\Psi_x'+\Psi_z^*\Psi_z')]^2}{1-b^2(|\Psi_x|^2+|\Psi_z|^2)}\Psi_x\right\} \tag{4a}$$

$$\Psi_z'=\frac{-b}{(1-b^2)^{1/2}}(1-|\Psi_x|^2-|\Psi_z|^2)\Psi_x , \tag{4b}$$

 ©1991 The American Physical Society

where the normalized fields $\Psi_x$ and $\Psi_z$ are related to the actual ones by $\Psi_x = e_x\sqrt{n_2/n_0}/b$ and $\Psi_z = -ie_z\sqrt{n_2/n_0}/b$, the prime denotes differentiation with respect to the normalized transverse coordinate $X = kn_0bx$, $k$ is the wave number in free space, Re indicates taking the real part, and the waveguide height is defined as

$$b = (1-\beta^2/k^2n_0^2)^{1/2} , \tag{5}$$

the magnitude of which determines the degree of coupling between the components $\Psi_x$ and $\Psi_z$. The decoupling occurs only when $b$ approaches zero. This then leads to $\Psi_z = 0$ and Eq. (4) reduces to

$$\Psi_x'' + \Psi_x - |\Psi_x|^2\Psi_x = 0 , \tag{6}$$

which is in fact the wave equation governing the normalized field $\Psi_y$ of the TE mode provided that $\Psi_x$ is replaced by $\Psi_y = e_y\sqrt{n_2/n_0}b$.

Now consider first the solutions for this special case. The solutions to Eq. (6) can in general be written as

$$\Psi_x(X) = f(X)\exp[ih(X)] , \tag{7}$$

where $f(X) = |\Psi_x(X)|$ and $h(X)$ are real functions. Substitution of this expression into Eq. (6) plus some algebraic manipulation leads to the solitary wave solutions (Appendix)

$$\Psi_x(X) = f_{\max}[1 - A^2\mathrm{sech}^2(f_{\max}AX/\sqrt{2})]^{1/2}[ih(X)] , \tag{8a}$$

$$h(X) = \pm\{f_{\min}X/\sqrt{2} + \tan^{-1}[(f_{\max}^2/f_{\min}^2 - 1)^{1/2} \times \tanh(f_{\max}AX/\sqrt{2})]\} , \tag{8b}$$

where $f_{\max} = |\Psi_x(\pm\infty)|$ and $f_{\min} = |\Psi_x(0)|$ are the maximum and minimum values of $|\Psi_x(X)|$ related by

$$2f_{\max}^2 + f_{\min}^2 = 2 \tag{9a}$$

and

$$A = (1 - f_{\min}^2/f_{\max}^2)^{1/2} . \tag{9b}$$

The case of $A = 1$ (or $f_{\min} = 0$) is referred to as the dark spatial solitary wave (Fig. 1), whereas $A < 1$ is referred to as the gray spatial solitary waves (Fig. 1). As defined [10], the spatial solitary waves are the solutions of the wave equation obeying $|\Psi_x(X)| \to \text{const}$, $\Psi_x'(X) \to 0$ and $\Psi_x''(X) \to 0$ as $X \to \mp\infty$, i.e., the evolution of the field starts and ends up at the equilibrium points of the equation. This condition $\Psi_x''(X) \to 0$ as $X \to \mp\infty$ applied to Eq. (6) yields

$$|\Psi_x(\pm\infty)| = f_{\max} = 1 \text{ or } 0 . \tag{10a}$$

But $f_{\max} = 0$ means $\Psi_x(X) \equiv 0$. Thus the only physical solution for the spatial solitary wave is $f_{\max} = 1$, which inserted into Eq. (9a) yields

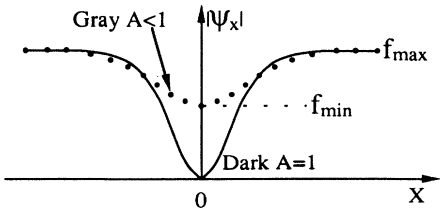


FIG. 1. Schematic illustration of solitary wave solutions of Eq. (8).

$$|\Psi_x(0)| = f_{\min} = 0 \text{ and } A = 1 . \tag{10b}$$

Accordingly, we conclude that the self-defocusing nonlinear medium of a Kerr-law type can only support the dark spatial solitary wave, or no gray spatial solitary waves can possibly exist in such a nonlinear medium.

This conclusion seems contradictory to the work of Ref. [10]. But one must be aware that the existence of gray spatial solitary waves of the TE type predicted in Ref. [10] was based on the solutions to the nonlinear Schrödinger equation which is a consequence of the slowly varying approximation of the wave equation (2). The stationary solutions of the gray spatial solitary waves predicted in Ref. [10] appear no longer possible when the term involving the second derivative with respect to $z$ is retained in the wave equation.

## III. PHASE-SPACE ANALYSIS

In the special case of $b \to 0$, Eq. (4) [or Eq. (6)] is shown only to yield the dark solitary wave solution and the normalized fields are real functions. This is also true for general cases of $b > 0$. Thus we take $\Psi_x$ and $\Psi_z$ to be real. Equation (4) can then be written alternatively in the form of the two first-order differential equations

$$\Psi_x' = \frac{b}{1-b^2(3\Psi_x^2+\Psi_z^2)} \times \left[2b\Psi_x\Psi_z' + (1-b^2)^{1/2}\left[\frac{1}{b^2} - \Psi_x^2 - \Psi_z^2\right]\right]\Psi_z , \tag{11a}$$

$$\Psi_z' = \frac{-b}{(1-b^2)^{1/2}}(1-\Psi_x^2-\Psi_z^2)\Psi_x . \tag{11b}$$

It can be shown that the system of Eq. (11) possesses an invariant

$$\frac{b^2}{1-b^2}(1-\Psi_x^2-\Psi_z^2)^2\Psi_x^2 + \frac{1}{b^2}\Psi_z^2 + \Psi_x^2 - \tfrac{1}{2}(\Psi_x^2+\Psi_z^2)^2 = \Gamma = \text{const} , \tag{12a}$$

which can be written in an explicit form

$$\Psi_z^2=\frac{1}{2b^2\Psi_x^2/(1-b^2)-1}\left\{-\frac{1}{b^2}+\frac{2b^2\Psi_x^2(1-\Psi_x^2)}{1-b^2}+\Psi_x^2 \pm\left[\left\{\frac{1}{b^2}-\frac{2b^2\Psi_x^2(1-\Psi_x^2)}{1-b^2}-\Psi_x^2\right\}^2 -4\left\{\frac{b^2\Psi_x^2}{1-b^2}-\frac{1}{2}\right\}\left\{\frac{b^2\Psi_x^2(1-\Psi_x^2)^2}{1-b^2}+\Psi_x^2-\frac{\Psi_x^4}{2}-\Gamma\right\}\right]^{1/2}\right\}. \tag{12b}$$

Plotted on the $\Psi_x-\Psi_z$ phase space, this equation yields an infinite set of trajectories associated with the solutions to Eq. (11). Illustrated in Fig. 2 are the characteristics of the trajectories for $0<b<1\sqrt{3}$ ($\approx 0.58$) in (a), $0.58<b<0.82$ in (b), and $0.82<b<1$ in (c). Although the trajectory characteristics in Figs. 2(a)–2(c) are qualitatively different, they all possess five singular points

$$(\Psi_x,\Psi_z)=(0,0)\ , \tag{13a}$$

$$(\Psi_x,\Psi_z)=(\pm 1,0)\ , \tag{13b}$$

$$(\Psi_x,\Psi_z)=(\pm 1/\sqrt{3}b,0)\ , \tag{13c}$$

surrounded by enclosed curves or run through by a separatrix. The singularities are the points at which the slope of the $\Psi_x-\Psi_z$ curves becomes indeterminate, i.e.,

$$\frac{d\Psi_x}{d\Psi_z}=\frac{0}{0}\ , \tag{14}$$

which leads to Eq. (13) upon substitution of Eq. (11).

The shape of the trajectories determines the characteristic of solutions. Enclosed curves are associated with periodic solutions while open trajectories represent growing or decaying solutions (i.e., $\Psi_z\to\pm\infty$ and $\Psi_x\to$const or $\Psi_x\to\pm\infty$ as $X\to\pm\infty$). The solitary waves are related to the separatrix when it passes through the equilibrium points (where $\Psi_x'=\Psi_z'=0$ giving rise to $d\Psi_x/d\Psi_z=0/0$, i.e., an equilibrium must be a singularity but not necessary conversely) identified as the starting or the terminating points at $X\to\mp\infty$ of the field evolution. This appears only in Fig. 2(a) for the trajectory marked with arrows. But when a separatrix runs through singularities which are not the equilibrium points (i.e., at these points $d\Psi_x/d\Psi_z=0/0$ but $\Psi_z'\neq 0$ or $\Psi_x'\neq 0$) such as the trajectory marked with arrows passing through singularities $(\Psi_x,\Psi_z)=(\pm 1\sqrt{3}b,0)$ in Fig. 2(b), the separatrix is then associated with a periodic solution. Recall that the solitary wave is defined as $\Psi_x\to$const and $\Psi_z\to$const as $X\to\pm\infty$ or $\Psi_x'=\Psi_z'=0$ as $X\to\pm\infty$ at which the system comes to rest. The points at which $\Psi_x'=\Psi_z'=0$ are referred to as equilibrium points of the system. For Eq. (11), there are three equilibrium points $(\Psi_x,\Psi_z)=(0,0)$ and $(\pm 1,0)$ which are run through by the separatrix in Fig. 2(a). The points $(\Psi_x,\Psi_z)=(\pm 1/\sqrt{3}b,0)$ passed through by the separatrix in Fig. 2(b) are singularities ($d\Psi_x/d\Psi_z=0/0$) arising from the singularities of Eq. (11a). At these points, $\Psi_x'=d\Psi_x/dX=0/0$ leading to $d\Psi_x/d\Psi_z=0/0$ but $\Psi_z'\neq 0$. Therefore $(\pm/\sqrt{3}b,0)$ in Fig. 2(b) do not correspond to the starting or the terminating points at which the system is at rest, but $(\pm 1,0)$ in Fig. 2(a) do. It follows from this analysis that the solitary waves can possibly exist only within $0<b<1/\sqrt{3}$, equivalent to $\sqrt{2/3}n_0$ ($\approx 0.82n_0$) $<\beta/k<n_0$.

## IV. DARK SPATIAL SOLITONS OF THE TM TYPE

By solving Eq. (11) numerically, it is found that the dark spatial solitary waves of the TM type can indeed exist within $0<b<1/\sqrt{3}$, confirming the prediction from the phase-space analysis. Figure 3 illustrates the normal-

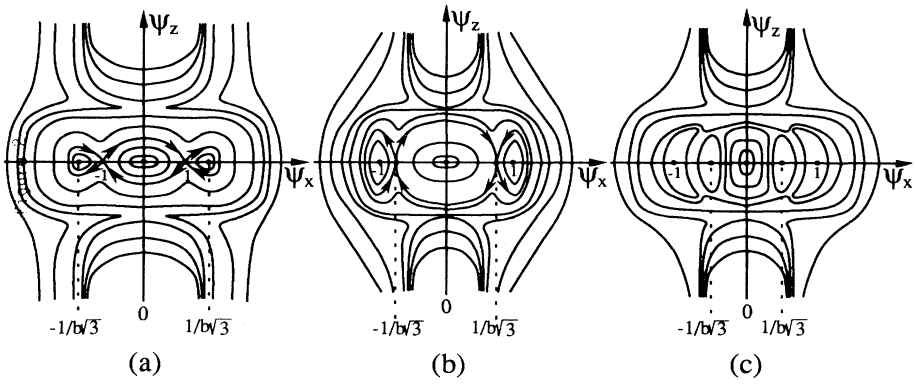


FIG. 2. Characteristics of the trajectories on the $\Psi_x-\Psi_z$ phase space for (a) $0<b<1/\sqrt{3}$ ($\approx 0.58$), (b) $0.58<b<0.82$, and (c) $0.82<b<1$.

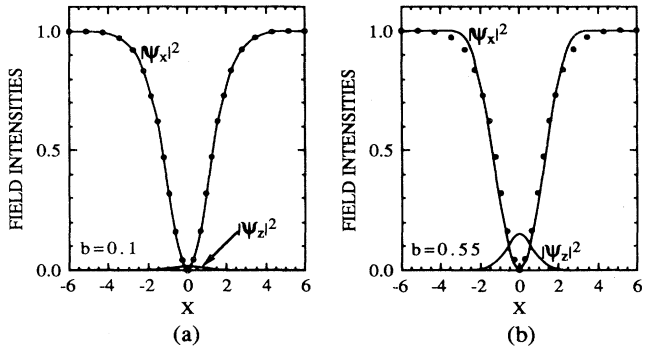


FIG. 3. Intensity profiles of the dark spatial solitary waves of the TM type for waveguide heights $b=0.1$ in (a) and $b=0.55$ in (b). The curve composed of large solid circles delineates the field intensity profile of the TE dark spatial solitary wave.

ized field intensity profiles for various $b$. Recall that the dark spatial solitary waves of the TE type can exist across the whole range of the wave effective index $n_{\text{eff}}=\beta/k$ from 0 to $n_0$, in contrast with the TM dark spatial solitary wave which can exist within $0.82n_0<n_{\text{eff}}<n_0$ only, almost five times as narrow as that of the TE type. The difference in the self-trapping behavior between the TE and TM types here is due to the presence of the longitudinal component $\Psi_z$ (or $e_z$) which tends to exaggerate defocusing thus lessens the self-guidance. And this defocusing effect of the $\Psi_z$ component becomes significant when $b$ is large. This is shown in Fig. 3 for the field intensity profiles and in Fig. 4 for the corresponding self-induced index profiles of the TM wave together with the TE wave (identified by the curve of large solid circles) for comparison.

One impressive feature revealed from Fig. 3 is that the longitudinal component $\Psi_z$ of the TM wave has a bright intensity profile. This bright intensity induces an extra hole index profile which inclines to counterbalance the convex index profile created by the dark intensity profile

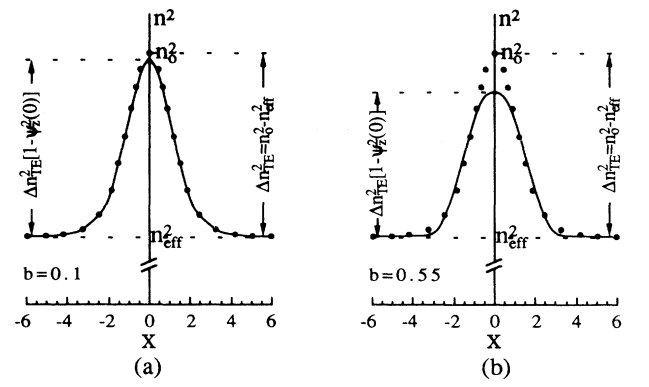


FIG. 4. Induced index profiles $n^2=n_0^2-n_0n_2|\mathbf{E}|^2=n_0^2[1-b^2(\Psi_x^2+\Psi_z^2)]$ corresponding to the intensity profiles of Fig. 3.

of the transverse component and thus belittles the self-focusing induced by the transverse component. See, for instance, Figs 3(a) and 4(a) where the refractive index $n_x^2$ induced by the transverse component $\Psi_x^2$ is indistinguishable from that for the TE wave delineated by the curve composed of large solid circles but the total induced index including the contribution from the longitudinal component is weakened compared with $n_x^2$. This defocusing effect is strengthened with increasing $b$ since the intensity of the bright longitudinal component increases with increasing $b$ as shown in Fig. 3 and in the following analytic relation between the peak intensity $\Psi_z^2(0)$ of the longitudinal component and the waveguide height $b=(1-n_{\text{eff}}^2/n_0^2)^{1/2}$:

$$\Psi_z^2(0)=[1-(1-b^4)^{1/2}]/b^2 , \tag{15}$$

which is derivable from Eq. (12) by specifying $\Gamma=\frac{1}{2}$ corresponding to the separatrix. This peak intensity is in fact directly related to the peak-induced index height by (Fig. 4)

$$\Delta n_{\text{TM}}^2=(n_0^2-n_{\text{eff}}^2)[1-\Psi_z^2(0)]=\Delta n_{\text{TE}}^2[1-\Psi_z^2(0)] , \tag{16}$$

which decreases with increasing $\Psi_z^2(0)$ and thus with increasing $b$. Here $\Delta n_{\text{TE}}^2=n_0^2-n_{\text{eff}}^2$ is the peak-induced index for the TE wave. Therefore, on the one hand, as indicated in Fig. 3 or Eq. (15), the bright field distribution of the longitudinal component gradually manifests itself with increasing $b$ and hence poses a growing demand for the induced refractive index to support. On the other hand, the self-guidance based on the induced refractive index is attenuated with increasing $b$ [as seen from Eq. (16) and Fig. 4]. Apparently, when $b$ augments to a certain extent exceeding the critical value of $1/\sqrt{3}$, the longitudinal component then becomes so intense but the induced refractive index is so weakened that the induced weak index profile can no longer bear the strongly guided longitudinal component. Accordingly, the self-guidance becomes impossible.

Another interesting characteristic of the TM wave disclosed in Fig. 4 is its propagation at cutoff. As illustrated, the wave effective index $n_{\text{eff}}=\beta/k$ of the TM wave is always equal to the minimum value of the induced index profile in spite of the fact that its longitudinal component behaves like a bright solitary wave. This is the same as the TE wave.

But in contrast to the TE case, the field intensity profile shape of the transverse component $\Psi_x$ varies with the waveguide height $b$, deviating from the $\tanh^2 X/\sqrt{2}$ function of the TE wave as shown in Fig. 3. Consequently, this change of field shape with varying $b$ leads to a change in power carried by the wave.

For a bright spatial solitary wave, the power, defined as $P=\frac{1}{2}\text{Re}\int_{A_\infty}\mathbf{E}\times\mathbf{H}^*dA$ with $\mathbf{H}$ the magnetic field, is a finite quantity. However, for a dark spatial solitary wave, this is a divergent quantity because of the constant intensity background. Accordingly, we define the hole power by the finite quantity

$$P_{\text{hole}}=\tfrac{1}{2}\text{Re}\int_{A_\infty}(\mathbf{E}_{\max}\times\mathbf{H}_{\max}^*-\mathbf{E}\times\mathbf{H}^*)dA ,$$

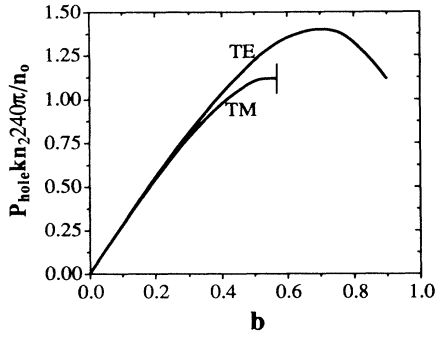


FIG. 5. Normalized hole power $P_{\text{hole}}kn_2240\pi/n_0$ for trapping the TM and Te type dark spatial solitons vs waveguide height $b$.

where $\mathbf{E}_{\max}$ and $\mathbf{H}_{\max}$ are the values of $\mathbf{E}$ and $\mathbf{H}$ at $|X|=\infty$. Figure 5 illustrates the hole power as a function of waveguide height $b$ for TM and TE dark spatial solitons. In both cases, the hole power increases with increasing $b$ when $b<0.71$, but $P_{\text{hole}}$ for TE increases faster than that for TM. This indicates that the TM wave requires slightly higher real power to support than that for TE.

Theoretically, an infinite power would be needed to form the proper constant background for a dark soliton to propagate, thus hampering experimental realization. This difficulty, however, can be overcome by approximating the constant background with a finite-width bright background (such as a Gaussian background) as done in Refs. [12–14]. The dark wave would not "feel" any difference between the constant background and a finite-width background provided that the background width is much larger than the dark soliton width.

## V. CONCLUSION

In summary, the dark spatial solitons of the TM type are predicted to exist in the self-defocusing nonlinear medium within the range of the wave effective index from $0.82n_0$ to $n_0$, in contrast to the TE type which exists over the range of $n_{\text{eff}}$ from 0 to $n_0$. The field profile of the TM spatial soliton is also shown to depend on the wave effective index $n_{\text{eff}}$, deviating from the hyperbolic tangent function of the TE type with decreasing $n_{\text{eff}}$

## APPENDIX

Equation (6), decomposed into two real coupled equations, reads

$$fh''+2f'h'=0 , \tag{A1}$$

$$f''-fh'^2+f-f^3=0 , \tag{A2}$$

upon substituting Eq. (7) into Eq. (6) and separating into real and imaginary parts. Direct integration of Eq. (A1) yields

$$h'=I_1f^2 , \tag{A3}$$

where $I_1$ is a constant. This equation, inserted into Eq. (A2) which is then integrated leads to

$$f'^2=\tfrac{1}{2}f^4-f^2-\frac{I_1^2}{f^2}+I_2 , \tag{A4}$$

with $I_2$ a constant. This directly gives the solutions for $f$ in an integral form

$$X=\pm\int\frac{df}{\left[\frac{1}{2}f^4-f^2-\frac{I_1^2}{f^2}+I_2\right]^{1/2}}+I_3 . \tag{A5}$$

The solutions (A5) are in general oscillatory, expressible in terms of elliptical functions. The solitary wave solutions occur only when the integration constants $I_1$ and $I_2$ are related to the maximum and minimum values $f_{\max}$ and $f_{\min}$ of $f$ by

$$2I_1^2=f_{\max}^4f_{\min}^2 , \tag{A6}$$

$$2I_2=f_{\max}^2(f_{\max}^2+2f_{\min}^2) , \tag{A7}$$

plus the condition of Eq. (9a). Substitution of these conditions into (A5) immediately results in

$$f=f_{\max}[1-A^2\operatorname{sech}^2(f_{\max}AX/\sqrt{2})]^{1/2} , \tag{A8}$$

which then, substituted into Eq. (A3), gives $h(X)$ in Eq. (8b).

[1] R. Y. Chiao, E. Garmire, and C. H. Townes, Phys. Rev. Lett. **13**, 479 (1964).
[2] H. A. Haus, Appl. Phys. Lett. **8**, 128 (1966).
[3] D. I. Abakrov, A. A. Akopyan, and S. I. Pekar, Zh. Eksp. Teor. Fiz. **52**, 463 (1967) [Sov. Phys.—JETP **25**, 303 (1967)].
[4] V. E. Zakharov and A. B. Shabat, Zh. Eksp. Teor. Fiz. **61**, 118 (1971) [Sov. Phys.—JETP **34**, 62 (1972)].
[5] A. Barthelemy, S. Maneuf, and C. Froehly, Opt. Commun. **55**, 193 (1985).
[6] S. Maneuf, R. Desailly, and C. Froehly, Opt. Commun. **65**, 193 (1988).
[7] S. Maneuf and F. Reyneud, Opt. Commun. **66**, 325 (1988).
[8] J. S. Aitchison, A. M. Weiner, Y. Silberberg, M. K. Oliver, J. L. Jackel, D. E. Leaird, E. M. Vogel, and P. W. Smith, Opt. Lett. **15**, 471 (1990).
[9] Y. Chen, Electron. Lett. **27**, 380 (1991).
[10] V. E. Zakharov and A. B. Shabat, Zh. Eksp. Teor. Fiz. **64**, 1627 (1973) [Sov. Phys—JETP **37**, 823 (1973)].
[11] Y. Chen and A. W. Snyder, Electron. Lett. **27**, 565 (1991).
[12] D. R. Andersen, D. E. Hooton, G. A. Swartzlander, and A. E. Kaplan, Opt. Lett. **15**, 783 (1990).

[13] G. R. Allan, S. R. Skinner, D. R. Andersen, and A. L. Smirl, Opt. Lett. **16**, 156 (1991).
[14] G. A. Swartzlander, D. R. Andersen, J. J. Regan, H. Yin, and A. E. Kaplan, Phys. Rev. Lett. **66**, 1583 (1991).
[15] A. W. Snyder, D. J. Mitchell, and L. Poladian, Opt. Lett. **16**, 21 (1991).
[16] T. Tamir, *Integrated Optics* (Springer-Verlag, Berlin, 1979).
[17] A. W. Snyder and J. D. Love, *Optical Waveguide Theory* (Chapman and Hall, London, 1983).